communications chemistry

ARTICLE

https://doi.org/10.1038/s42004-021-00453-x OPEN

Direct observation of knock-on reaction with umbrella inversion arising from zero-impact-parameter collision at a surface

Matthew J. Timm [1,2], Lydie Leung[1,2], Kelvin Anggara [1] & John C. Polanyi [1✉]

In Surface-Aligned-Reactions (SAR), the degrees of freedom of chemical reactions are restricted and therefore the reaction outcome is selected. Using the inherent corrugation of a Cu(110) substrate the adsorbate molecules can be positioned and aligned and the impact parameter, the collision miss-distance, can be chosen. Here, substitution reaction for a zero impact parameter collision gives an outcome which resembles the classic Newton's cradle in which an incident mass 'knocks-on' the same mass in the collision partner, here $F + CF_3 \rightarrow (CF_3)' + (F)'$ at a copper surface. The mechanism of knock-on was shown by Scanning Tunnelling Microscopy to involve reversal of the CF_3 umbrella as in Walden inversion, with ejection of (F)′ product along the continuation of the F-reagent direction of motion, in collinear reaction.

[1] Lash Miller Chemical Laboratories, Department of Chemistry, University of Toronto, Toronto, ON, Canada. [2] These authors contributed equally: Matthew J. Timm, Lydie Leung. ✉email: john.polanyi@utoronto.ca

With the advent of quantum mechanics[1], it became evident that partially-formed bonds could stabilize the transition state, facilitating chemical reaction. Using this formalism H. Eyring and M. Polanyi plotted the potential energy surface for a collinear reaction $H+H_2 \rightarrow H—H—H \rightarrow H_2+H$, in which the intermediate configuration was the transition state stabilized by the presence of collinear extended H—H bonds[2].

Early attempts to gain experimental information concerning the geometry of transition states began with the scattering of directed gaseous reagent atoms from dipolar molecules aligned in electric fields[3–5]. Important insights into reaction dynamics between gaseous molecules were obtained from crossed molecular beams, however, these studies averaged over all impact parameters, precluding control of the collision geometry[6]. The adsorption of reagents on a surface has allowed the collision geometry to be varied by "Surface-Aligned-Reaction", SAR[7–9]. Scanning tunneling microscopy (STM) has provided direct information on molecular alignment in surface reactions[10–13]. A recent extension of SAR employing STM achieved a high degree of directionality in reactive collisions, employing the ordered surface-atoms as a collimator of energetic reagent "projectiles"[14,15]. These projectiles were formed by electron-induced dissociation of chemisorbed precursor molecules so that the projectiles collided with fixed chemisorbed "target" molecules at selected impact parameters, *b*. The impact parameter is defined as the perpendicular distance to the center-of-mass of the target molecule at the closest approach[14].

In the present work, the projectile is an F-atom, the target a chemisorbed CF_3 and the selected impact parameter $b = 0 \pm 0.5$ Å. Here STM shows that an efficient substitution reaction yields a product (F)′-atom "knocked-on" from the CF_3 along the continuation of the collision-direction. The CF_3 is shown, directly by STM, to invert its CF_3 umbrella as the reagent F displaces the product (F)′ in the collinear "knock-on" reaction. Substitution with retention of collision-direction in the transition state indicates that the dynamics involve one-dimensional reaction, as proposed in early work on the classic substitution reaction, $H+H_2 \rightarrow H_2+H$, and in the widely used concept of Walden inversion[16].

Results and discussion

Alignment on the surface. The adsorption and reaction of individual chemisorbed CF_3 molecules at a Cu(110) surface at 4.6 K has been previously examined by STM and density functional theory (DFT) calculations[14,15]. The CF_3 molecule binds atop a Cu atom through its C-atom, giving a tetrahedral configuration (Fig. 1a). Two of the C–F bonds are tilted away from the copper surface by 31°, termed the raised CF_2 end of CF_3. The third C–F bond is tilted only 10° out of the surface plane, pointed along $[1\bar{1}0]$. This almost in-plane C–F bond is seen by STM to be the one that breaks in electron-induced reaction[14]. The backside of the CF_3 adsorbate is composed of the raised CF_2 and the Cu atom below, as highlighted by the black dashed triangle in the side view of Fig. 1a. The F reagent will be shown to attack the backside of CF_3, which opens as the CF_3 inverts.

High-contrast imaging of a single chemisorbed CF_3 at 4.6 K, obtained by scanning at a bias close to the Fermi level with a functionalized STM tip[17–21], is shown in Fig. 1a (and Supplementary Fig. 1a). The distinction between the CF_2 and CF ends of CF_3 is visible in the height-profile of Fig. 1a, from a to b along the $[1\bar{1}0]$ direction (see Supplementary Note 1). The measured slope on the left-hand side of the height-profile, S1, is steeper than that on the right-hand side, S2. The steeper slope (S1: |0.36| Å/Å) corresponds to the backside of the CF_3 adsorbate (triangle, Fig. 1a).

The electron-induced dissociation of CF_3 yields a difluorocarbene (CF_2) 18.0 Å to the left of the CF_3 reagent position (shown by a white cross in Fig. 1) and an F-atom 3.7 Å to the right along

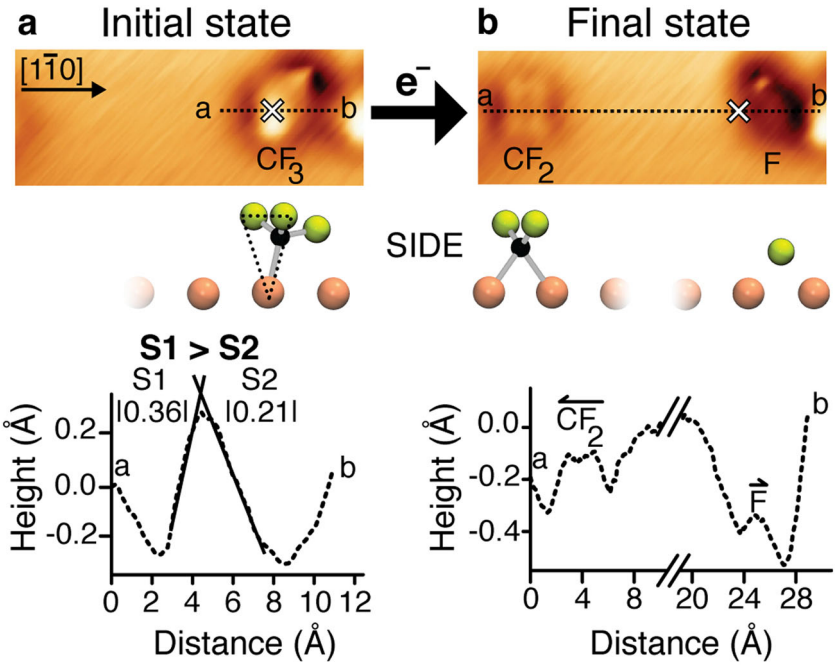

Fig. 1 Electron-induced dissociation of chemisorbed CF_3 gives directed CF_2 and F. a The high-contrast STM image (30 Å × 12 Å, $I = 1.0$ nA, $V = -5$ mV) of a single CF_3 chemisorbed at the Cu(110) surface, in which the backside of the CF_3 is shown to face to the left of the image, is highlighted by a black dashed triangle in the side view. The height-profile of the CF_3 reagent is taken along $[1\bar{1}0]$ from **a** to **b**. The slopes indicated on this line profile are S1 = |0.36 ± 0.02| Å/Å and S2 = |0.21 ± 0.01| Å/Å. **b** The electron-induced dissociation of the CF_3 shows long-range recoil of the dissociation product CF_2 to the left and a short-range recoil of F to the right of the white cross in the STM image, both along a $[1\bar{1}0]$ copper row. The height-profile of the two products, **a**–**b**, is taken along $[1\bar{1}0]$. The white cross overlaid upon each STM image marks the initial position of the CF_3 prior to dissociation.

the [1$\bar{1}$0] direction (Fig. 1b). These recoil distances agree with those previously reported for the two products[15]. The locations of the CF_2 and F-atom products from the CF_3 dissociation show that the alignment of the CF_3 umbrella is correctly assigned with the raised CF_2 end at the left.

Electron-induced reaction. The "knock-on" reaction is initiated by electron-induced dissociation of a chemisorbed CF_3 (Fig. 2). The CF_3, shown at the left in Fig. 2a, is termed the "precursor" of CF_2 and of F. The atomic F, coming from CF_3, recoils along the Cu-row and collides with a second chemisorbed CF_3, the 'target' at the right in Fig. 2a, to give an inverted CF_3 umbrella $(CF_3)'$ and a knocked-on F-atom (F)′. The initial state comprised a pair of chemisorbed CF_3 on the same Cu-row, separated by 5.17 ± 0.06 Å (Fig. 2a). The adsorption configuration shown in Fig. 2a was the only one observed for a pair of CF_3. The asymmetry identified in the height-profile of a single CF_3 is also observed in the a–b height-profile of each CF_3 of the pair. The CF_3 precursor and CF_3 target exhibit the same tilted configuration, with the backside at the left (Fig. 2a). This implies that the in-plane C–F bond of the CF_3 precursor is directed toward the backside of the CF_3 target molecule. This adsorption configuration of the CF_3 pair agrees with the simulated STM image obtained from the calculated geometry (Supplementary Fig. 2a).

Electron addition to the CF_3 precursor gave three products, chemisorbed CF_2, $(CF_3)'$, and (F)′ on the same Cu-row (Fig. 2b and Supplementary Fig. 2b). As in Fig. 1, the CF_2 and F-atom products are shown to the left and right sides of the initial position of the CF_3 reagent. The F-atom travels 8.94 ± 0.04 Å, seemingly passing through the chemisorbed CF_3 target. The (F)′ is formed as the result of a zero impact parameter collision between the F-atom reagent and the CF_3 target. The F-atom reagent has displaced an (F)′-atom product from the target (the displaced product atom is highlighted by the blue circle in Fig. 2). The (F)′ product recoiled along the continuation of the direction of approach of the F-atom reagent, hence being designated as "knocked-on". Concurrently, the $(CF_3)'$ is displaced 1.0 Å to the left of the prior CF_3 target position, with its umbrella inverted compared with its original alignment in Fig. 2a. This umbrella inversion is clearly evidenced by the reversed S1:S2 ratio in the height-profile (from S1 < S2 to S1 > S2).

Knock-on reaction is found for 46 of the 71 cases of F + CF_3 collision (65 ± 10%). Figure 3 shows the observed positions of the

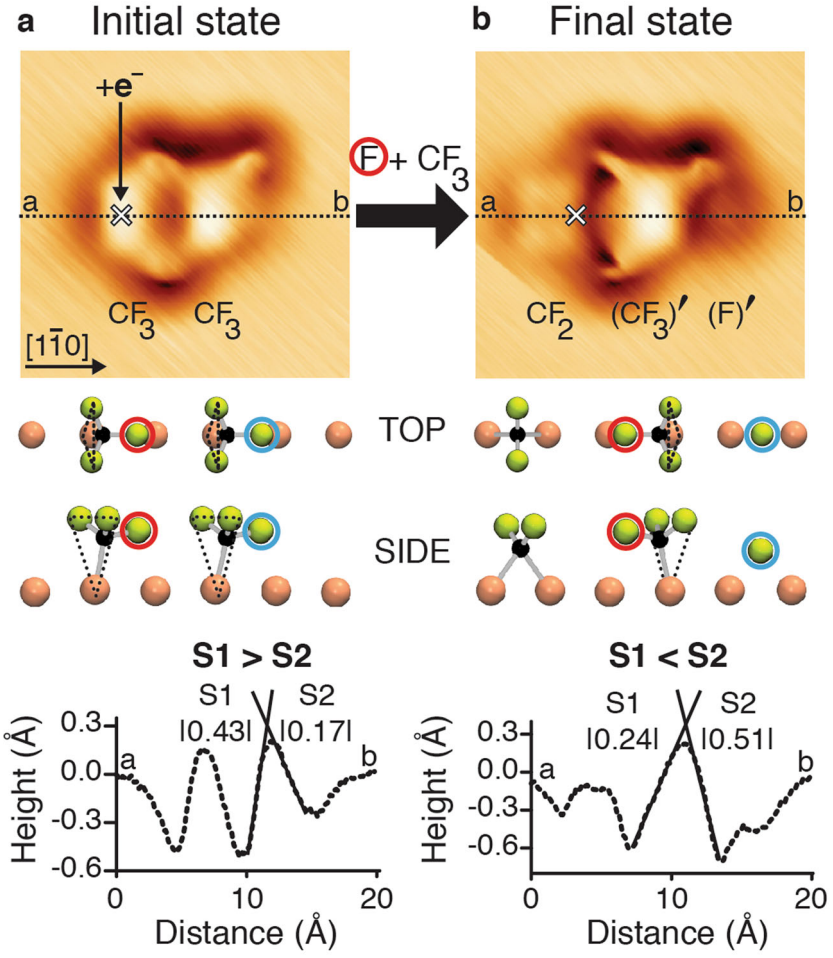

Fig. 2 "Knock-on" reaction: F plus CF_3 gives $(CF_3)'$ plus (F)′. a The STM image (20 Å × 20 Å, I = 0.1 nA, V = −1 mV) of the initial state of a pair of CF_3 molecules, chemisorbed at the Cu(110) surface, before electron addition to the CF_3 "precursor" molecule at the left (location marked by the white cross). In the side view, below, both CF_3 are oriented with their backsides at the left (black dashed triangles). In the top and side views (lines two and three), the F-atom at the tip of the CF_3 umbrella of the precursor is circled in red and in blue for the CF_3 target. **b** The final state STM image (20 Å × 20 Å, I = 0.1 nA, V = −1 mV) shows the three products of the electron-induced reaction: CF_2, $(CF_3)'$ and (F)′. In the top and side views, the CF_3 and $(CF_3)'$ are seen to have an inverted umbrella. The height-profiles (bottom panels) are measured along [1$\bar{1}$0] from **a** to **b**. The measured slopes of the CF_3 target in **a** are S1 = |0.43 ± 0.02| Å/Å and S2 = |0.17 ± 0.01| Å/Å. Those of the $(CF_3)'$ in **b** are S1 = |0.24 ± 0.01| Å/Å and S2 = |0.51 ± 0.01| Å/Å.

knock-on reaction products, $(CF_3)'$ and (F)′, relative to the initial position of the CF_3 precursor (white cross). The data are folded such that the initial state is the same as in Fig. 2, with the origin at the location of the CF_3 precursor. Dissociation of the CF_3 precursor yields two oppositely recoiling products, CF_2 and F. We define the recoil direction of the F-atom reagent as the "forward" direction ($\vec{F}$ FORW). As the CF_2 recoils backward, we did not consider it to be a part of the knock-on reaction. This CF_2 is found to recoil a wide variety of distances along the Cu-row, uncorrelated with knock-on. The distance distribution of all the reaction products is shown in Supplementary Fig. 3a. A striking feature of the $(CF_3)'$ and (F)′ knock-on products is that they are collinear with the incoming reagent F. This indicates that the linear momentum of the projectile is retained throughout the existence of the transition state.

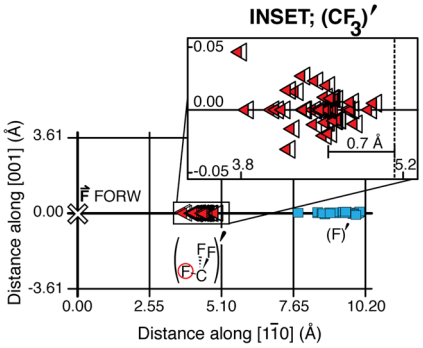

Fig. 3 Product distribution, $(CF_3)'$ and (F)′, from knock-on reaction with umbrella inversion. Final positions of the products of reaction, following collision of the reagent F-atom with the adjacent CF_3 target. The reagent F-atom was formed by electron-induced dissociation of a CF_3 precursor. The two reaction products are chemisorbed $(CF_3)'$ shown as red-tipped triangles, and (F)′ product shown as blue squares. A schematic of the inverted $(CF_3)'$ with the F-atom circled in red is shown below in the figure. The scale corresponds to the unit-cell dimensions of the Cu(110) surface. An enlarged view of the distribution of the $(CF_3)'$ products is shown in the inset. The lateral spread in the inset is < ± 2 % of the distance between the rows. The location of the CF_3 target is marked by a dashed line. The (F)′ product (blue squares) is found on the copper row, along with the continuation of the 'forward' direction of the incoming F-atom marked '$\vec{F}$ FORW'.

From the CF_3 precursor position, the $(CF_3)'$ product (red-tipped triangles in Fig. 3) is observed at an average distance of 4.50 ± 0.07 Å and the (F)′ product (blue squares) at 9.44 ± 0.08 Å. An enlarged view of the $(CF_3)'$ distribution is given in the inset to Fig. 3. For each case of knock-on reaction the $(CF_3)'$ is displaced slightly backwards from the CF_3 target position (dashed line). The displacement is found to be 0.67 ± 0.07 Å on average, and invariably coincides with inversion of the CF_3 umbrella in the target. This displacement is observed in each case of inversion, where the STM resolution allows the umbrella alignment to be obtained (50% of cases). The second product of knock-on reaction, (F)′ was found to have traveled ~4.27 Å past the CF_3 target, along the continuation of the direction of the F-atom reagent.

In a minority of cases (25 out of 71 cases: 35 ± 7 %), a different outcome is observed; "unsuccessful" knock-on (Supplementary Fig. 3b and Supplementary Note 2). The F-atom reagent is found to have scattered in the backward direction from the CF_3 target, rather than forward. In this "unsuccessful" knock-on the CF_3 target was not observed to undergo inversion, nor was it observed to be displaced from its initial position.

Previous studies of electron-induced dissociation of CF_3 have reported, in addition to travel along a Cu-row, lateral travel of F-atom products to an adjacent Cu-row. This was attributed, through molecular dynamics calculations, to in-plane rotation of the intact CF_3. Computation showed that a rotation of < 7° was sufficient to account for the observed lateral travel of the F-atom[15]. A rotation of the CF_3 precursor by 7° increases the impact parameter to $b = 0.5$ Å, providing a valuable upper limit for the miss-distance that permits knock-on reaction. The fact that $b > 0.5$ Å, which favors orbital motion, gives no observable knock-on product, indicates that knock-on is not due to orbiting of the projectile around the target. Instead, the system provides a direct path (Fig. 4), over a low energy barrier, leading from incoming F to out-going (F)′.

Knock-on mechanism. To obtain the mechanism of collision between the reagent F-atom and the CF_3 target at zero impact parameter, a climbing image-nudged elastic band (CI-NEB) calculation was performed[22,23]. The initial and final states correspond to those observed by STM in Fig. 2. From this CI-NEB calculation, the successive configurations of the reagents are identified as the system progresses along the reaction coordinate.

The knock-on reaction shown in Fig. 4 takes place across two successive barriers. The first barrier involves the dissociation of

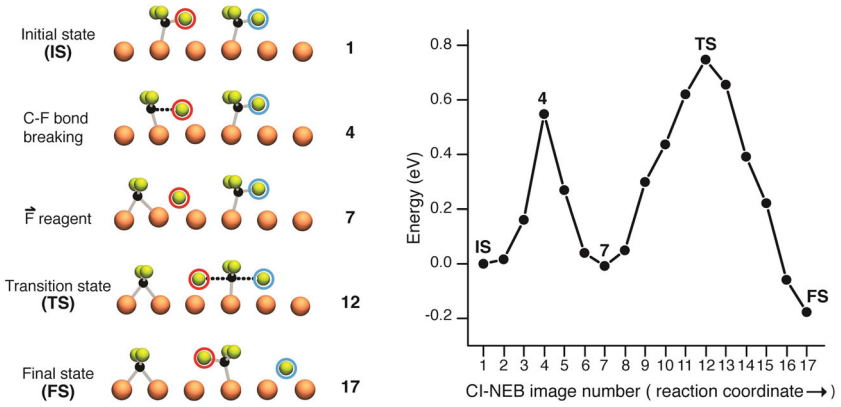

Fig. 4 Climbing image-nudged elastic band (CI-NEB) pathway for knock-on reaction. Minimum-energy pathway across a DFT potential energy surface as obtained from a CI-NEB calculation. Five representative CI-NEB images along the pathway are shown at the left of the figure. In the initial state, IS, the CF_3 precursor is at the left and the CF_3 target is at the right. The F-atom, originating in the CF_3 precursor, is marked by a red circle, whereas the (F)′ product is marked by a blue circle.

the CF_3 precursor to produce CF_2 and an F-atom—the latter circled in red. This first barrier of 0.55 eV is required for the extension of the in-plane C–F bond (image 4). Following C–F bond breaking, the CI-NEB shows CF_2 and F at the nearest adsorption sites. For the F-atom this is the short-bridge site beneath, whereas for the CF_2 fragment it is the short-bridge site 1.6 Å away (image 7).

The second barrier of the CI-NEB results from the energized F-atom projectile (red) colliding with the CF_3 target, and thereafter ejecting an (F)′ (blue). The barrier for this F-atom substitution is 0.76 eV required to form the symmetric linear transition state, F—CF_2—(F)′ (Fig. 4, image 12). This arises from F attacking the backside of the chemisorbed CF_3 target, as in Walden inversion[16]. Following this, the CF_3 umbrella completes its inversion and knocks-on an (F)′-atom, which is repelled to its final position 3.7 Å away (Fig. 4, images 13–17). The small computed barrier, ~1 eV, accords with the high probability of 65% observed for knock-on. The mechanism derived from the CI-NEB supports knock-on occurring through a linear transition state with collinear ejection of (F)′ along the continuation of the direction of the incoming projectile.

Conclusions

In this work, we have examined the novel realm of "zero impact parameter" (zero collision miss-distance) chemistry, as an innovative means to control the scattering of reaction products at metal surfaces. We have shown that reaction at zero impact parameter occurs for the most part collinearly in one-dimension (1D), while inverting the target molecule as in classic Walden inversion, seen directly here. Notably, the reaction products are expelled collinearly with the reagent motion in what we term "knock-on" dynamics. The new concept is that reduced dimensionality in reagent motion leads, through momentum conservation, to reduced dimensionality in product motion. The appearance of 1D reaction is that an energized reagent, the "projectile", has passed through the "target" molecule to emerge collinearly on the other side. The consequence for chemistry is that the reagent energy can be passed on in successive collinear collisions, leading to a "knock-on chain". In a world where energy is to be conserved, these are favorable dynamics. This resembles the conservation of linear momentum that underlies the motion in Newton's cradle, knocking on a succession of steel balls.

Methods

STM. Experiments were performed with an LT-UHV Scanning Tunneling Microscope (Omicron) at 4.6 K. The Cu(110) surface was prepared by repeated cycles of Argon sputtering and annealing to 800 K. Tungsten STM tips were electrochemically etched in 3M NaOH solution. Functionalization of the STM tip was accomplished by positioning the tip above clusters of CF_3 and I-atom adsorbates and repeatedly performing −5 to −10 V pulses without identifying the species transferred to the tip. Functionalization of the tip was confirmed when the apparent height of the chemisorbed CF_3 was 3× greater than that obtained for a non-functionalized tip at the previous imaging conditions[14,15]. All STM images were taken at 4.6 K using constant current mode with the bias referred to the sample. CF_3 was obtained by dosing trifluoroiodomethane, CF_3I, onto the cleaned Cu(110) at 79.5 K, which dissociated upon adsorption. Then the crystal was cooled down to 4.6 K in the STM stage. The electron-induced dissociation of CF_3 was performed by (i) placing the tip over the adsorbate, (ii) adjusting the tip height, (iii) turning off the feedback loop, and (iv) ramping the sample bias to V_{pulse} (between 1.3 and 1.8 V). Dissociation was confirmed by imaging the products in a subsequent scan. The distance and direction of the dissociation products were analyzed using the WSxM Software[24].

DFT calculations. The DFT calculations were performed using the Vienna Ab initio Simulation Package (VASP)[25,26] on the SciNet supercomputer Niagara cluster[27,28]. The calculations used the projector augmented wave method[29,30] and the generalized gradient approximation (GGA) with the Predew-Burke-Ernzerhof functional[31]. Grimme's semi-empirical dispersion correction was added to correct for Van der Waals interactions[32]. The energy cutoff for the plane-wave basis set was 400 eV. The Cu(110) surface was modeled by a (3 × 10) slab consisting of 150 Cu atoms in five layers, separated with a 17 Å vacuum layer. All atoms were allowed to move except for the bottom two layers of Cu atoms, which were frozen. The adsorption geometries were obtained by relaxing the system until the force on each unfrozen atom was >0.01 eV/Å. The relaxation calculations were performed using a single Γ-point *k*-mesh sampling. Molecular structures were visualized using the Visual Molecular Dynamics software[33]. Simulated STM images and height-profiles were obtained through calculations using the Tersoff-Hamann approximation[34], and visualized using the Hive software[35,36].

CI-NEB calculations. The CI-NEB calculations were performed in VASP based on DFT using Γ-point only. Between the initial and final states calculated from the experimental data shown in Fig. 2, a local minimum was found along the reaction coordinate. This local minimum corresponds to CI-NEB image 7. This local minimum was relaxed following the same procedure as the initial and final states. To determine the barrier between the initial state and the local minimum, we used five images. A total of nine images were used to find the barrier between the local minimum and the final state. The calculations were conducted until the forces orthogonal to the band were <0.02 eV/Å. The Fast Inertial Relaxation Engine optimizer[37] was used to minimize the forces. To achieve convergence a time step of 0.01 (in 10.18 fs units) was used, instead of the time step previously employed[38].

Data availability

The data that support the findings of this study are available from the corresponding author upon reasonable request.

Received: 10 November 2020; Accepted: 18 January 2021;
Published online: 12 February 2021

References

1. London, F. Probleme der modernen Physik. 104–113 (S. Hirzel, Leipzig, 1928).
2. Eyring, H. & Polanyi, M. On simple gas reactions. *Z. Physikal. Chem. B* **12**, 279–311 (1931).
3. Brooks, P. R. & Jones, E. M. Reactive scattering of K atoms from oriented CH_3I molecules. *J. Chem. Phys.* **45**, 3449–3450 (1966).
4. Brooks, P. R. Molecular beam reaction of K with oriented CF_3I. Evidence for harpooning? *J. Chem. Phys.* **50**, 5031–5032 (1969).
5. Beuhler, R. J. & Bernstein, R. B. Crossed-beam study of the reactive asymmetry of oriented methyl iodide molecules with rubidium. *J. Chem. Phys.* **51**, 5305–5315 (1969).
6. Pan, H., Liu, K., Caracciolo, A. & Casavecchia, P. Crossed beam polyatomic reaction dynamics: recent advances and new insights. *Chem. Soc. Rev.* **46**, 7517–7547 (2017).
7. Bourdon, E. B. D. et al. Photodissociation, photoreaction and photodesorption of adsorbed species. Part 2.—CH_3Br and H_2S on LiF(001). *Faraday Discuss. Chem. Soc.* **82**, 343–358 (1986).
8. Tripa, C. E. & Yates, J. T. Jr. Surface-aligned reaction of photogenerated oxygen atoms with carbon monoxide targets. *Nature* **398**, 591–593 (1999).
9. Vaida, M. E. & Bernhardt, T. M. *Ultrafast Phenomena in Molecular Sciences.* Ch.10 (eds. de Nalda, R. & Bañares, L.) 231–261 (Springer, Cham, 2014).
10. Lauhon, L. J. & Ho, W. The initiation and characterization of single bimolecular reactions with a scanning tunneling microscope. *Faraday Discuss.* **117**, 249–255 (2000).
11. Maksymovych, P., Sorescu, D. C., Jordan, K. D. & Yates, J. T. Jr. Collective reactivity of molecular chains self-assembled on a surface. *Science* **322**, 1664–1667 (2008).
12. Kumagai, T. et al. H-atom relay reactions in real space. *Nat. Mater.* **11**, 167–172 (2012).
13. Ning, Z. & Polanyi, J. C. Surface aligned reaction. *J. Chem. Phys.* **137**, 91706 (2012).
14. Anggara, K., Leung, L., Timm, M. J., Hu, Z. & Polanyi, J. C. Approaching the forbidden fruit of reaction dynamics: aiming reagent at selected impact parameters. *Sci. Adv.* **4**, eaau2821 (2018).
15. Anggara, K., Leung, L., Timm, M. J., Hu, Z. & Polanyi, J. C. Electron-induced molecular dissociation at a surface leads to reactive collisions at selected impact parameters. *Faraday Discuss* **214**, 89–103 (2019).
16. Ingold, C. K. *Structure and Mechanism in Organic Chemistry* (Ithaca Cornell University Press, New York, 1969).
17. Temirov, R., Soubatch, S., Neucheva, O., Lassise, A. C. & Tautz, F. S. A novel method achieving ultra-high geometrical resolution in scanning tunnelling microscopy. *N. J. Phys.* **10**, 053012 (2008).
18. Weiss, C. et al. Imaging Pauling repulsion in scanning tunneling microscopy. *Phys. Rev. Lett.* **105**, 086103 (2010).
19. Han, Z. et al. Imaging the halogen bond in self-assembled halogenbenzenes on silver. *Science* **358**, 206–210 (2017).

20. Jelínek, P. High resolution SPM imaging of organic molecules with functionalized tips. *J. Phys. Condens. Matter* **29**, 343002 (2017).
21. Lawrence, J. et al. Combining high-resolution scanning tunnelling microscopy and first-principles simulations to identify halogen-bonding. *Nat. Commun.* **11**, 2103 (2020).
22. Henkelman, G., Uberuaga, B. P. & Jónsson, H. A climbing image nudged elastic band method for finding saddle points and minimum energy paths. *J. Chem. Phys.* **113**, 9901–9904 (2000).
23. Henkelman, G. & Jónsson, H. Improved tangent estimate in the nudged elastic band method for finding minimum energy paths and saddle points. *J. Chem. Phys.* **113**, 9978–9985 (2000).
24. Horcas, I. et al. WSXM: software for scanning probe microscopy and a tool for nanotechnology. *Rev. Sci. Instrum.* **78**, 013705 (2007).
25. Kresse, G. & Hafner, J. Ab initio molecular dynamics for liquid metals. *Phys. Rev. B.* **47**, 558–561 (1993).
26. Kresse, G. & Furthmüller, J. Efficient iterative schemes for ab initio total-energy calculations using a plane-wave basis set. *Phys. Rev. B.* **54**, 11169–11186 (1996).
27. Loken, C. et al. SciNet: lessons learned from building a power-efficient top-20 system and data centre. *J. Phys. Conf. Ser.* **256**, 12026 (2010).
28. Ponce, M. et al. Deploying a Top-100 supercomputer for large parallel workloads: the Niagara supercomputer. *Proceedings of the Practice and Experience in Advanced Research Computing on Rise of the Machines.* **34**, 1–8 (Association for Computing Machinery, New York, 2019).
29. Blöchl, P. E. Projector augmented-wave method. *Phys. Rev. B.* **50**, 17953–17979 (1994).
30. Kresse, G. & Joubert, D. From ultrasoft pseudopotentials to the projector augmented-wave method. *Phys. Rev. B.* **59**, 1758–1775 (1999).
31. Perdew, J. P., Burke, K. & Ernzerhof, M. Generalized gradient approximation made simple. *Phys. Rev. Lett.* **77**, 3865–3868 (1996).
32. Grimme, S., Antony, J., Ehrlich, S. & Krieg, H. A consistent and accurate ab initio parametrization of density functional dispersion correction (DFT-D) for the 94 elements H-Pu. *J. Chem. Phys.* **132**, 154104 (2010).
33. Humphrey, W., Dalke, A. & Schulten, K. VMD: visual molecular dynamics. *J. Molec. Graph.* **14**, 33–38 (1996).
34. Tersoff, J. & Hamann, D. R. Theory of the scanning tunneling microscope. *Phys. Rev. B* **31**, 805–813 (1985).
35. Vanpoucke, D. E. P. & Brocks, G. Formation of Pt-induced Ge atomic nanowires on Pt/Ge(001): a density functional theory study. *Phys. Rev. B* **77**, 241308 (2008).
36. Vanpouke, D. *HIVE STM-program—The Delocalized Physicist*; https://dannyvanpoucke.be/hive-stm-en/.
37. Bitzek, E., Koskinen, P., Gähler, F., Moseler, M. & Gumbsch, P. Structural relaxation made simple. *Phys. Rev. Lett.* **97**, 170201 (2006).
38. Sheppard, D., Terrell, R. & Henkelman, G. Optimization methods for finding minimum energy paths. *J. Chem. Phys.* **128**, 134106 (2008).

Acknowledgements

This work was funded in part by the Natural Sciences and Engineering Research Council of Canada (NSERC) and the University of Toronto NSERC General Research Fund. Theoretical calculations were performed on the Niagara cluster at SciNet HPC Consortium. SciNet is funded by the Canada foundation for innovation under the auspices of Compute Canada, the Government of Ontario, Ontario Research Fund-Research Excellence and the University of Toronto. K.A. thanks the Connaught International Scholarship for Doctoral Students for financial support.

Author contributions

All authors designed the project. M.J.T., L.L., and K.A. performed the experiments. L.L. and M.J.T. analyzed the data. M.J.T. conducted the ab initio calculations. M.J.T., L.L., and J.C.P. wrote the manuscript. All authors discussed the results and commented on the manuscript.

Competing interests

The authors declare no competing interests.

Additional information

Supplementary information The online version contains supplementary material available at https://doi.org/10.1038/s42004-021-00453-x.

Correspondence and requests for materials should be addressed to J.C.P.

Reprints and permission information is available at http://www.nature.com/reprints

Publisher's note Springer Nature remains neutral with regard to jurisdictional claims in published maps and institutional affiliations.